S.O. Zelinskyi, N.G. Stryzhakova, O.V. Gozhenko, Y.A. Maletin

HOW THE ELECTROCHEMICAL IMPEDANCE SPECTROSCOPY CAN DEEPEN THE UNDERSTANDING OF SUPERCAPACITOR PERFORMANCE

Institute for Sorption and Problems of Endoecology, NAS Ukraine
13 General Naumov Str., Kyiv, 03164, Ukraine, E-mail: s.o.zelinskyy@nas.gov.ua

Electrochemical impedance spectroscopy has been used for the characterization of electric double layer capacitors also known as supercapacitors. Specific surface area and pore size distribution for supercapacitor electrode materials and the results of impedance spectroscopy measurements for two types of commercially available nanoporous activated carbons and two graphene-type materials have been studied and compared with the results obtained from cyclic voltammetry and galvanostatic charge-discharge cycling the supercapacitor prototypes in different voltage ranges and at different current densities. It has been found that the results for the characteristics of studied supercapacitor prototypes differ insignificantly if they were obtained by different methods, while all three research methods have shown the advantage of materials with nanoporous activated carbon over materials of the graphene type. Besides, according to the data obtained by measuring impedance at low frequencies the deviations from ideal capacitive behaviour are more significant in case of graphene-type materials. Comparison of the three research methods used in this work shows that the method of impedance spectroscopy makes it possible to obtain the most complete and reliable information on the performance characteristics of the supercapacitor system, since not only the capacitance and resistance values, but their frequency dependence, as well as deviations (in degrees) from the purely capacitive vertical line at Nyquist plots and capacitance dissipation can be determined and taken into consideration.

Keywords: supercapacitors, electrochemical impedance spectroscopy, complex capacitance, cyclic voltammetry, galvanostatic cycling

INTRODUCTION

Electric double layer capacitors or supercapacitors (SC) are energy storage devices comprising two nanoporous carbon electrodes applied on metal current collectors, separated by a porous insulating film (separator) and immersed in a liquid electrolyte [1–3]. The energy stored in a SC depends mostly on its electrode pore structure and surface area accessible for the electrolyte to form the electric double layer. The SC internal resistance and, hence, the power density and efficiency depend on the conductivity of electrode components and electrolyte, in particular, on the degree of ion mobility (or diffusion) slowdown in nanopores. Various electrochemical methods are employed to measure the key SC characteristics, such as capacitance C and internal resistance R. The commonly used are cyclic voltammetry (CV) and galvanostatic (GS) charge-discharge cycling, though they are time-consuming and may affect the device characteristics [2, 4–6]. Electro-chemical impedance spectroscopy (EIS) is another technique to measure both capacitance

and resistance values at various voltages as well as some other SC characteristics but with a negligible impact on the system [7–13].

In EIS a periodic voltage or current signal is applied at various frequencies. Usually, the signal has a sine waveform of low amplitude and the corresponding response signal is registered. Most often the input signal is a small alternative voltage of 5–10 mV resulting in AC pulses near imposed or set DC potential. A small alternative signal is chosen to provide the pseudo-linear response of the same frequency for input and output signals. The main difference between them is an amplitude and shift in phase. The ratio of voltage (input signal) to current (output signal) in full complex view is the impedance denoted as Z:

$$Z(\omega) = \frac{U(\omega)}{I(\omega)} = |Z|e^{-i\varphi}. \qquad (1)$$

So impedance is just a form of full resistance that depends on frequency. The frequency ($f = \omega/2\pi$) is changed in a wide range, normally, from 10 mHz to 100 kHz. Complex values of Z form a numerical matrix and represent the behavior of a real Z_i' and imaginary Z_i'' parts of the

full system resistance and a phase shift φ at a certain frequency ω_i:

$$\begin{cases} Z[Z_i'; Z_i''; \omega_i], \ (i = 1,2,3, \dots N) \\ \qquad \varphi = \text{arctg}\left(\dfrac{Z_i''}{Z_i'}\right) \end{cases} \qquad (2)$$

The entire spectrum consists of a set of ranges; each of them can be described by a physical/chemical process occuring and set out by linear elements (R – fixed resistor, C – ideal capacitor, and L – ideal inductor) or nonlinear elements (W – Warburg or diffusion elements, CPE – constant phase element, *etc.*) [14–15].

This work aims at studying the EIS spectra of SC prototypes with four different electrode materials and comparing the results obtained with the corresponding SC characteristics found with the help of other techniques. Also the SC capacitance and resistance will be discussed as related with the total surface area and pore size distribution in the active electrode materials used.

EXPERIMENTAL

Type of materials for SC electrodes. The following nanostructured carbons have been studied:

• xGnPC750 graphene from XG Science, Inc. (USA), denoted below as xGN;

• C2087/rGOB006/Pw reduced graphene oxide from Graphenea (Spain), denoted below as rGO;

• YP50F activated carbon from Kuraray Chemical Co., Ltd (Japan), denoted below as YP5;

• YP80F activated carbon from Kuraray Chemical Co., Ltd (Japan), denoted below as YP8.

The first two graphene-type carbons have been developed as promising materials for SC technology. The YP5 and YP8 are already used by various SC manufacturers. Specific surface area and pore size distribution for rGO, YP5 and YP8 materials have been determined with the use of isotherms of nitrogen gas sorption–desorption at 77 K. The carbon specimens were kept in vacuum of $1 \cdot 10^{-4}$ Torr at 180 °C for 4 hours before the measurements with the use of NOVA2200 analyzer (Quantachrome, USA). Micro- and mesoporous structure was estimated by a DFT method, and the total surface area was evaluated by both DFT and BET methods that gave similar results for those three carbons. The porosity data for xGN have been taken from [16].

Prototype fabrication. SC electrodes comprising the carbon materials under study were manufactured by roller pressing the mixture of carbon powder with PTFE binder, the latter content being 7 % wt. The electrode tapes thus obtained were laminated onto aluminum foil of 20 micron thick as a current collector. To improve the conductivity and adhesion between the active electrode tape and the current collector the aluminum foil was preliminarily modified by the electric spark technique [17] that resulted in spot fusing the graphite particles into the foil surface and eliminating the native oxide layer therein. Besides, a thin layer of carbon black/PVDF mixture was applied onto the foil surface before the electrode lamination process. The electrode footprint was 30×50 mm and the electrode tapes of 100 μm thick were used except the xGN carbon where the electrode thickness was 200 μm and a footprint of 30×40 mm due to rather poor mechanical strength of a tape made of this material. The electrodes thus fabricated were dried in a vacuum for over 12 hours at 150 °C followed by assembling SC prototypes in a dry glove box. The prototypes comprised a pair of electrodes interleaved by a porous cellulosic separator (TF4530, Nippon Kodoshi), impregnated with electrolyte (1M Et$_4$NBF$_4$ in acetonitrile) and hermetically packed in a laminated aluminum shell.

SC characteristic measurements. Cycling voltammetry and electrochemical impedance spectroscopy measurements were carried out with Voltalab PGZ402; galvanostatic cycling was performed with Arbin Instrument BT2000 test bench.

For correct comparison of various electrode materials in SC prototypes, their specific characteristics will be used. The gravimetric capacitance (F/g) is the capacitance referred to the mass of active carbon material in one electrode. The internal resistivity (in $\Omega \cdot$cm^2) is the total resistance referred to 1 cm^2 of visible electrode area.

In experiments with galvanostatic (GS) charge-discharge cycles each prototype was cycled within a voltage range from $U_{\min}$ to $U_{\max}$. $U_{\max}$ varied from 1.5 to 2.7 V in 0.2–0.3 V steps. $U_{\min}$ was always chosen as half of $U_{\max}$. The cycling current started approximately from 10 mA$\cdot$cm^{-2} or 0.5 A$\cdot$g^{-1}and reached the value of 0.3 A$\cdot$cm^{-2}or 20A$\cdot$g^{-1}. Charge and discharge currents were the same (symmetrical mode) and repeated over eight cycles.

Cyclic voltammetry (CV) measurements were performed after completing the GS cycling

when a SC prototype reached the rated voltage and was fully charged. Three CV curves were recorded with a scan rate of 10 mV.s^{-1} from 2.7 to 0 V, and the last one was used to calculate the C_{CV} capacitance as in Eq. 3.

$$C_{CV} = \frac{I}{\Delta V/\Delta t} .\qquad(3)$$

EIS was the third method to measure the characteristics of SC prototypes under study. EIS measurements were carried out at a nominal voltage of 2.7 V in the frequency range from 10 mHz to 100 kHz with a disturbance voltage of a sinusoidal waveform with an amplitude of 5 mV. The angular frequency ($\omega = 2\pi f$) will be used to present the results below.
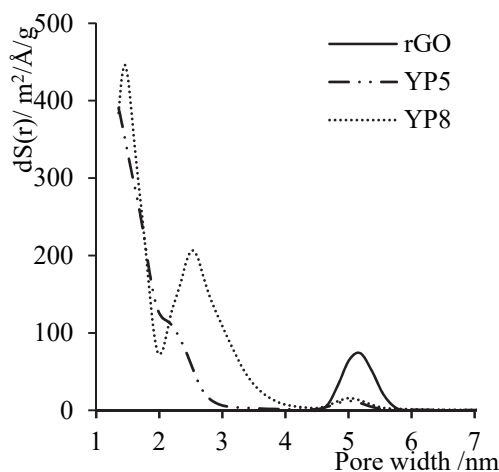
RESULTS AND DISCUSSION

Material porosity studies and electrode characteristics. The results for porosity studies are presented in Table 1 and Fig. 1. As can be seen from these data, the graphene-type materials have a predominantly mesoporous structure with their specific surface area much less than that of YP-type activated carbons. The latters have also a certain share of mesopores, though, near the boundary between micro- and mesoporosity.

Table 2 summarizes the main characteristics of electrodes manufactured from the materials under study.

Table 1. Specific surface and porosity of carbon materials under study

Carbon type	Total surface area, m^2/g	Micropore area, m^2/g	Mesopore area, m^2/g
rGO	446	–	446
xGN	738*	218*	520*
YP5	2180	1850	330
YP8	2420	1470	950

* as measured in [16]

**Fig. 1.** Increments of specific surface area *vs*. pore width for three selected carbons (DFT study)

Table 2. Characteristics of electrodes in SC prototypes

Carbon type	Thickness, μm	Footprint, mm	Electrode density, g/cc
rGO	100	30×50	0.64
xGN	200	30×40	0.73
YP5	100	30×50	0.65
YP8	100	30×50	0.49

Electrochemical test results.

Galvanostatic charge-discharge cycling (GS mode). This technique is most commonly used to evaluate the SC capacitance and internal resistance. Fig. 2 illustrates a unit GS charge-discharge cycle, and these curves were used to evaluate the characteristics of SC prototypes (herein with YP8 electrodes).
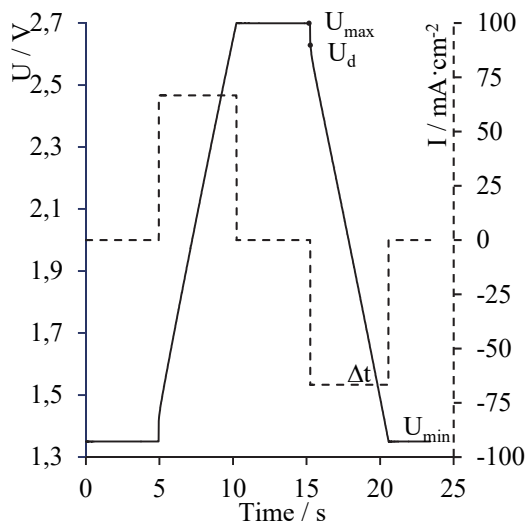
Fig. 2. Typical charge-discharge curves to evaluate the SC capacitance and resistance; solid line – voltage; dashed line – current density

The internal resistance, R_{GS} (in $\Omega \cdot cm^2$), was evaluated from the voltage drop (or IR-drop) when switching the discharge current, I, according to Eq. (4):

$$R_{GS} = \frac{U_{max} - U_d}{I} \qquad (4)$$

and the capacitance C_{GS} was evaluated from the discharge curve according to Eq. (5):

$$C_{GS} = \frac{I \cdot \Delta t \cdot S}{U_d - U_{min}} \qquad (5)$$

where I is the current in $A \cdot cm^{-2}$, S is the visible electrode area in cm^2, U_d is the voltage in 10 ms after switching the discharge process, U_{min} and U_{max} is the voltage range for cycling (see Fig. 2 captions).

The capacitance and resistance were evaluated in GS mode for each set of currents and voltages and the final values were calculated by the averaging procedure.

Fig. 3 illustrates plots of capacitance *vs.* current load for the prototypes under study. In our numerous measurements this plot is normally close to linear one at medium and high loads and, therefore, we usually use the linear extrapolation to zero current value to compare the maximum capacitance of various SC prototypes. This value will be denoted below as C_{GS}.

As has been found experimentally and illustrated in Fig. 3, the maximum current value for a SC prototype with rGO electrodes is about 80 $mA \cdot cm^{-2}$ while for prototypes with other electrode materials the current density can reach 250 $mA \cdot cm^{-2}$. This is obviously due to the high value of internal resistance for rGO-based prototype as compared with others – see in Fig. 4 *b*. As a result of that high resistance, a voltage drop (or *IR*-drop) becomes too substantial when switching the high current load, thus resulting in low efficiency and distorted capacitance evaluation.

Fig. 4 illustrates plots of capacitance, C_{GS} or internal resistance, R_{GS} *vs.* the maximum cycling voltage, U_{max}. The capacitance increases with an increase in voltage for activated carbons and rGO, and this effect is normally observed in SC systems due to the corresponding reduction of double electric layer thickness. A decrease in C_{GS} value with voltage for xGN graphene material is probably due to some degradation of the system with increasing the voltage. Fig. 4 also illustrates that SC prototypes with activated YP carbons in electrodes have higher capacitance and lower resistance than their analogs comprising

graphene-type materials. For all the prototypes the resistance value varies rather insignificant with voltage.

The resistance and capacitance obtained from GS mode will further be presented in Table 3 and discussed hereinafter.
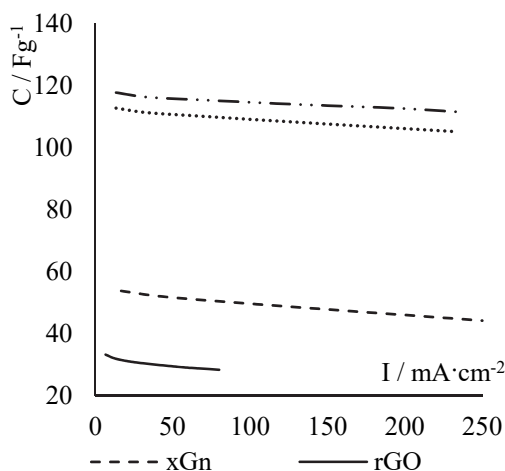
Fig. 3. Plots of capacitance density *vs*. current density for SC prototypes under study when cycling them between 1.35 and 2.7 V
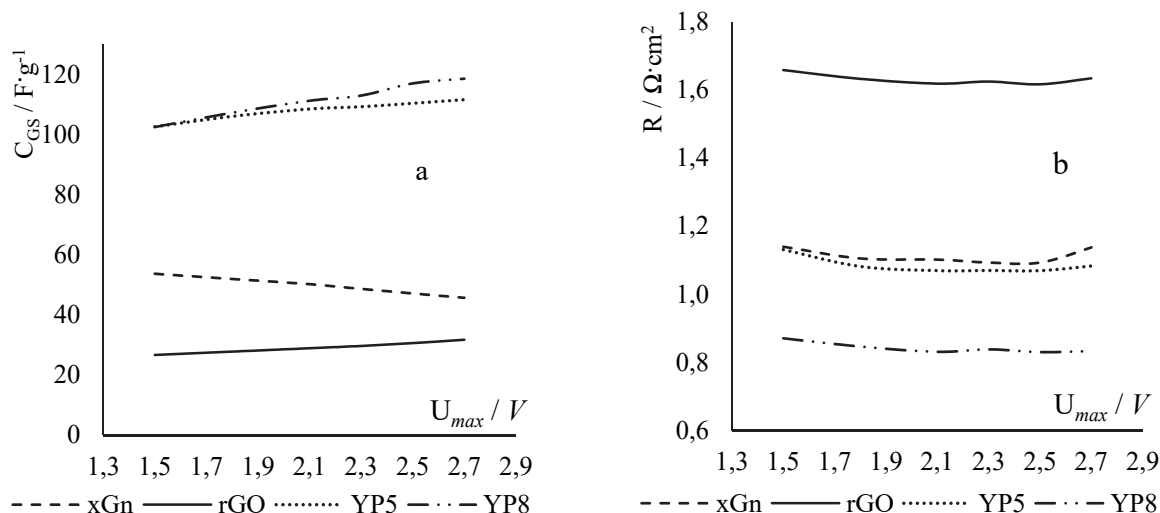
Fig. 4. Plots of specific capacitance (*a*) or resistance (*b*) *vs*. the maximum cycling voltage, U_{max}

Cyclic voltammetry (CV mode). Fig. 5 illustrates the CV curves in capacitance *vs*. voltage coordinates, and herein the capacitance increases with voltage for all SC prototypes under study including that with rGO electrodes. This contrast with the GS mode in Fig. 4 *a* may be referred to a short time needed to register a CV curve as compared with much longer charge-discharge cycling at various voltages. A practically linear increase in capacitance with voltage for YP carbons implies that the charging process is predominantly conditioned by the

formation of double electric layer in the electrode porous structure. The value of capacitance C_{CV} at the rated voltage of 2.7 V will be compared with the results of other techniques in Table 3.

Electrochemical impedance spectroscopy (EIS mode). Fig. 6 shows Nyquist (Z'' *vs*. Z') plots for SC prototypes under study.

All the curves have a similar shape, namely, demonstrate more or less vertical line at low frequencies and cross the horizontal axis in a point shifted to the left from the extrapolated quasi vertical line. If the ideally vertical line without

that shift were observed this would have meant a pure capacitive response and EIS spectra could be modeled by a single RC circuit with two linear elements. In this case the Z complex value is defined as:
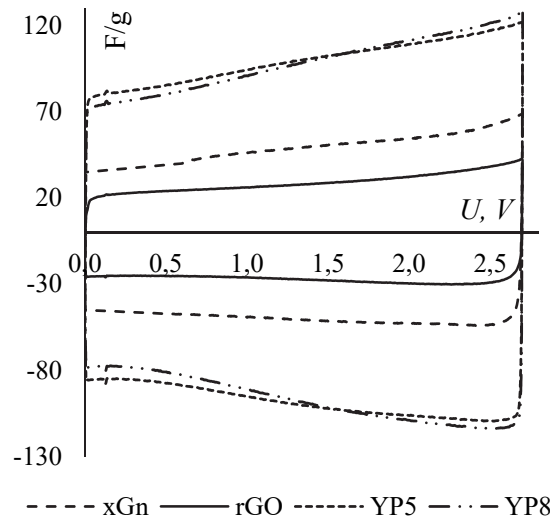
$$Z = R_{EDR} + \frac{1}{i\omega C_{EIS}}. \tag{6}$$

Fig. 5. CV curves in capacitance *vs.* voltage coordinates at 10 mV·s⁻¹ scan rate
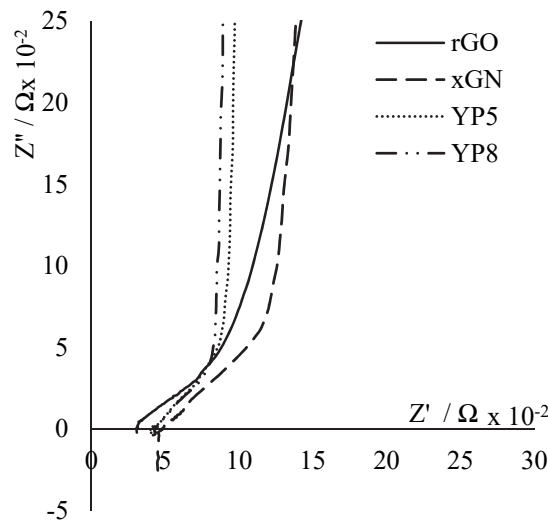

Fig. 6. Nyquist plots for SC prototypes under study

This model behaves as an ideal capacitor at low frequencies and a fixed resistor at high frequencies. Bode plot of a pure RC model must show a steep increase in $|Z|$ modulus with decreasing the frequency, where the major contribution to the total impedance comes from capacitance. The $|Z|$ modulus retains the same and equals R_{EDR} at high frequencies, where the capacitive contribution to impedance is negligible. The phase shift changes from –90° at low frequencies to 0° phase angle at high frequencies. In real systems the Bode plots demonstrate similar behavior, though, with more or less significant deviations - see in Fig. 7. Here we do not see a clear boundary or quantitative "knee" value, where capacitance or resistance has a predominant contribution to the EIS spectra. Besides, the phase shift can get a negative value

at high frequency and does not reach a constant value of –90° at low frequency or 0° at high frequency.

As a result, EIS spectra for the SC prototypes under study cannot be described with the use of a single RC circuit but at least one more term

should be added to the total impedance to take into account those deviations. Looking for an appropriate solution we have divided the EIS spectra obtained into three ranges as shown in Fig. 8.
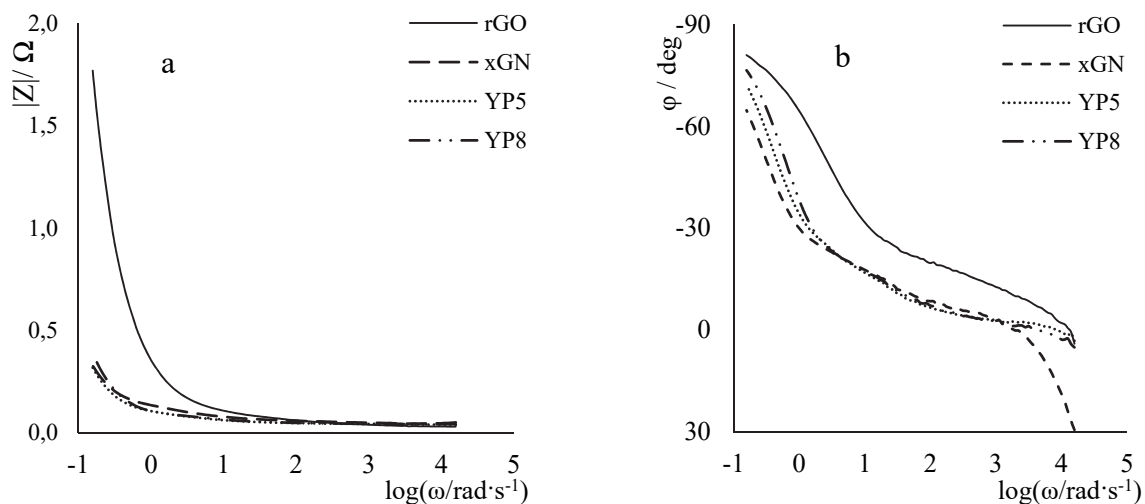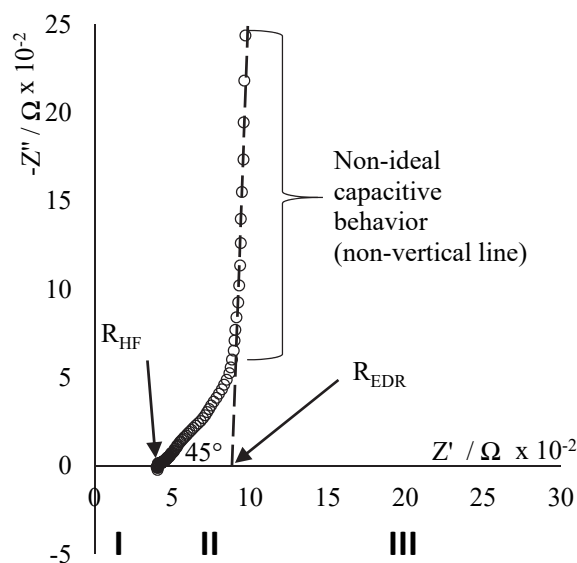
Fig. 7. Bode plots of four prototypes under study

Fig. 8. Three ranges of a typical Naquist plot (YP8 carbon as an example)

Here the total impedance of the systems is defined as:

$$Z = Z_{HF}(\omega) + Z_{MF}(\omega) + Z_{LF}(\omega), \qquad (7)$$

where $Z_{HF}(\omega)$ is the impedance in the high frequency range (**I**), $Z_{MF}(\omega)$ is the impedance in the medium frequency range (**II**), and $Z_{LF}(\omega)$ is the impedance in the low frequency range (**III**). Obviously, there are no clear boundaries between

these ranges either since each addend influences the impedance at all frequencies, though, the predominant contribution takes place in a certain range.

$Z_{HF}(\omega)$ contains two terms: inductive impedance $Z_L = i\omega L$ and ohmic resistance $Z_R = R_{HF}$ at high frequency. Inductive impedance enables to describe the negative phase shift in Bode plots (see Fig. 7) and positive values

of Z'' in the Nyquist plot (see Fig. 6). R_{HF} is the ohmic resistance defined as a resistance without any additives from the imaginary part, and thus, the R_{HF} is the crosspoint at the Z'-axis in the Nyquist plot [18, 19].

$Z_{LF}(\omega)$ also contains two terms and might have been described by a single RC circuit if a pure capacitive response took place. With the electrode materials under study, however, the low-frequency tails in the Nyquist plots are not really vertical - see Figs. 6 and 8. To describe that deviation a pure capacitance in Eq. 6 should be replaced by a constant phase element, CPE: $Z_{CPE}(\omega) = \frac{1}{Y(i\omega)^\alpha}$, where Y and α are frequency-independent parameters. The Y parameter becomes a pure capacitance provided α equals unit. A few theories have been proposed to account for the non-ideal behavior of the electric double layer capacitors, but none has been accepted [20–22]. In our case α is also an empirical constant without any physical basis. The R_{EDR} term in Eq. 6 is the sum of high frequency resistance R_{HF} with an additional term arising due to electrolyte distributed resistance in nanopores that increases with a decrease in frequency.

The medium frequency range described as $Z_{MF}(\omega)$ is the most difficult for analysis. A slope of –45 ° turning into a line close to vertical on the Nyquist plot can be described using various types of equivalent electrical circuits with linear and non-linear elements. The most popular model is based on the De Levie theory of rough electrode [23] and can be described either by an RC transmission line element (TLE), or by a few parallel RC circuits, or by "vertical ladder" network [13, 14, 24, 25] that give similar results. The entire process is most successfully modeled

by an RC transmission line. Sometimes this range is also associated with the impedance of Warburg diffusion, although the redox process accompanied by this diffusion does not occur, and, in principle, the Warburg element may not be taken into account when describing the SC.

It is worth noting that the full set of EIS spectral data can hardly be described by a single model. As mentioned above, in our approach the entire spectrum has been divided into three ranges followed by analyzing them individually. Some of the characteristics obtained from the investigated EIS spectra are listed in Table 3 – see approximate boundaries of ranges, various resistance and capacitance values, and deviations (in degrees) from a purely capacitive vertical line. To estimate the R_{EDR} value and the deviation from vertical line on the Nyquist plot, 10 points were selected at the lowest frequencies. The R_{GS} value obtained from galvanostatic mode lies between R_{HF} and R_{EDR}. The fourth resistance, R_{CC} was evaluated from the complex capacitance using the RC model – see Figs. 9 and 10 and their discussion below.

Table 3 also contains three capacitance values for each electrode material, and two of them, namely C_{GS} and C_{CV}, are widely used and discussed above. The third value, C_{EIS}, was obtained from the EIS spectra using the classical definition of capacitive impedance [7, 26] and taking into account that the complex capacitance is a vector with real and imaginary components as follows:

$$C = 1/i\omega Z = C'(\omega) + iC''(\omega), \qquad (8)$$

where $C'(\omega)$ is the useful capacitance related to the energy stored, and $C''(\omega)$ is associated with capacitance/energy dissipation.

Table 3. Comparison parameters obtained from various techniques

| Carbon type	Resistance, $\Omega \cdot cm^2$				Capacitance, $F \cdot g^{-1}$			Deviation from vertical line at low f, degrees	High freq. range. (I) f >~[kHz]	Low freq. range. (III) f < ~ [Hz]
	R_{GS}	R_{HF} f→0	R_{EDR} f→0	R_{CC}	C_{GS}	C_{CV}	C_{EIS} f→0			
rGO	1.6	0.5	2.3	1.5	32	42	21	7.0°	$2 \cdot 10^3$	10
xGN	1.1	0.7	1.8	1.6	57	71	53	6.3°	$2 \cdot 10^3$	1
YP5	1.1	0.6	1.2	1.3	112	122	116	2.0°	$4 \cdot 10^3$	1
YP8	0.8	0.6	1.1	1.1	119	127	123	2.3°	$4 \cdot 10^3$	1
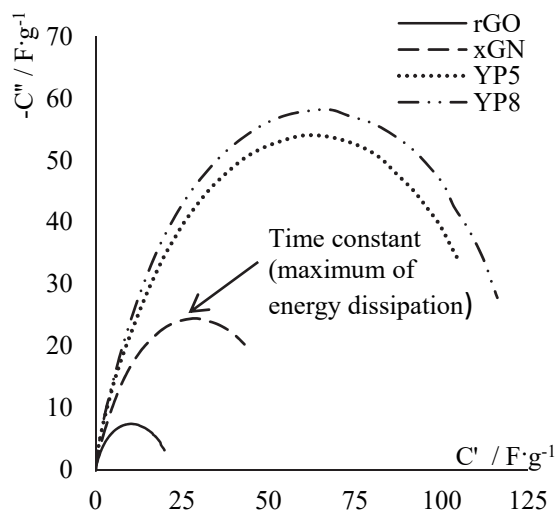
Fig. 9. Real and imaginary components of complex capacitance

The obvious regular semicircular curves in Fig. 9 suggest that capacitance can be described by a single RC model. According to this model, the complex capacitance is defined as [10]:

$$C = \frac{C}{1+\omega^2 R^2 C^2} - i \frac{\omega R C^2}{1+\omega^2 R^2 C^2}. \tag{9}$$

From this equation the C value at $\omega \to 0$ can be estimated, and the results obtained are very close to those observed at the lowest frequency (10 mHz in our experiments). The maximum values on the semicircles correspond to the maximum energy dissipation that takes place at $\omega = 1/RC$ and, hence, from these data the time

constants τ_{EIS} for SC prototypes under study can be evaluated using the relation $\tau_{EIS} = \omega^{-1}$, where ω is the cutoff frequency at the top of semicircles in Fig. 9 or from maxima of C'' *vs.* log (ω) in Fig. 10 *b*. Then the resistance values R_{CC} can be calculated using the equation $R_{CC} = \tau_{EIS}/C_{EIS}$, where C_{EIS} is the maximum capacitance at $\omega \to 0$ (Fig. 10 *a*). Both R_{CC} and C_{EIS} values thus obtained are shown in Table 3, and in our opinion they are more reliable than the values obtained by other methods and listed in there.
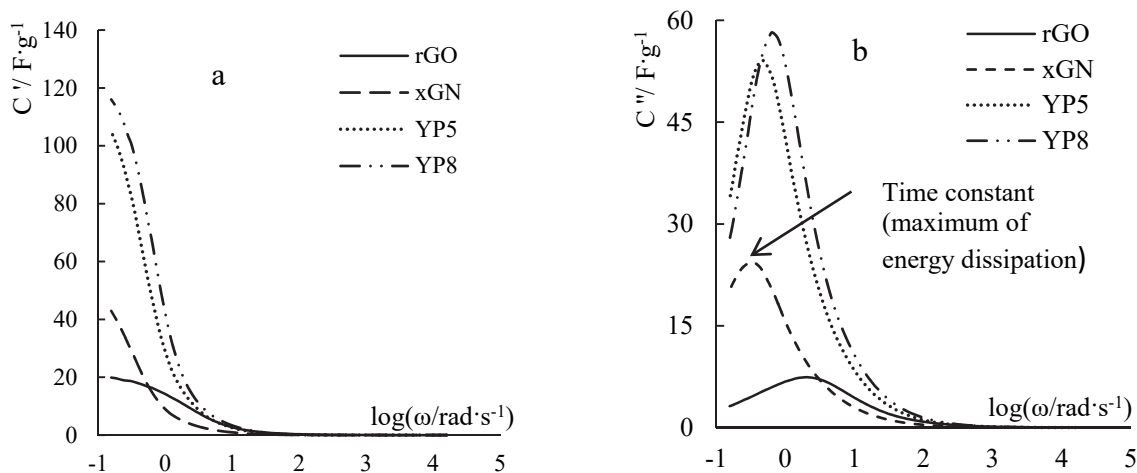
Fig. 10. C' (a) and C'' (b) *vs.* log ω dependences of SC prototypes

Table 4. Time constants derived from different techniques

Carbon type	τ_{GS}, s	τ_{EIS}, s
rGO	0.15	0.09
xGN	0.40	0.72
YP5	0.36	0.45
YP8	0.23	0.32

The time constant values evaluated from GS mode and from EIS are listed in Table 4. Higher deviations between τ_{EIS} and τ_{GS} for graphene-type materials (about 70–80 %) may be accounted for similar deviations in either capacitance or resistance (see in Table 3) and higher energy dissipation for these materials. Besides, graphene-type materials demonstrate larger deviation from the vertical line in the low-frequency range on the Nyquist plot and a bit different frequency behavior than YP carbons – see the last three columns in Table 3. An important note: the use of the complex capacitance obtained from the EIS measurements makes any RC circuit simulation unnecessary, since the experimental data can be directly used to estimate reliably the key SC characteristics.

CONCLUSIONS

• The electrochemical impedance spectroscopy (EIS) technique has been used to characterize the performance of electric double-layer capacitors or supercapacitors (SC), and the test results have been compared with those obtained from galvanostatic charge-discharge cycling and cyclic voltammetry.

• Two types of commercially available nanoporous active carbons and two graphene-type materials have been used in SC electrodes, and all three investigation methods have shown the advantage of activated carbon materials over graphene-type ones. In addition, according to EIS data, the deviations from capacitive behaviour are more significant in case of graphene-type materials.

• The EIS method provides the most comprehensive information about the performance of the SC, since not only capacitance and resistance values, but also their frequency dependence, deviations from purely capacitive behavior at low frequencies and capacitance dissipation can be obtained and taken into consideration.

Використання електрохімічної імпедансної спектроскопії для поглибленого вивчення характеристих суперконденсаторів

С.О. Зелінський, Н.Г. Стрижакова, О.В. Гоженко, Ю.А. Малетин

*Інститут сорбції та проблем ендоекології Національної академії наук України
вул. Генерала. Наумова, 13, Київ, 03164, Україна, s.o.zelinskyy@nas.gov.ua*

Методом електрохімічної імпедансної спектроскопії досліджено характеристики конденсаторів подвійного електричного шару, також відомих як суперконденсатори. Для двох типів комерційно доступних нанопоруватих вугільних матеріалів і двох графеноподібних матеріалів було визначено питому поверхню та розподіл пор за розмірами. Ці матеріали були використані в електродах макетів суперконденсаторів, для яких проведені вимірювання імпедансу. Одержані характеристики порівняні з результатами, отриманими методом гальваностатичного циклування і циклічної вольтамперометрії в широкому діапазоні напруги та при різних

густинах струму. Показано, що характеристики макетів, отримані різними методами, відрізняються несуттєво і встановлено, що нанопорувате активоване вугілля реалізує кращі характеристики в порівнянні з графеноподібними матеріалами. На основі даних імпедансної спектроскопії також показано, що відхилення при низьких частотах від ідеальної ємнісної поведінки більш суттєве для графеноподібних матеріалів, ніж для нанопоруватого вугілля. Порівняння трьох методів дослідження показало, що метод імпедансної спектроскопії дозволяє отримати найбільш повну та достовірну інформацію щодо характеристик суперконденсаторів, оскільки дає можливість отримати не лише ємність та опір, але також їхню частотну залежність. Крім того, можна визначити відхилення (в градусах) від чисто ємнісної вертикальної лінії в діаграмах Найквіста при низьких частотах та вклад розсіяної ємності, які слід враховувати для оцінки ефективності суперконденсатора.

Ключові слова: суперконденсатор, електрохімічна імпедансна спектроскопія, комплексна ємність, циклічна вольтамперометрія, гальваностатичне циклування

REFERENCES

1. Conway B.E. *Electrochemical Supercapacitors.* (New York: Kluwer Academic Publishers/Plenum Press., 1999).
2. Kötz R., Carlen M. Principles and applications of electrochemical capacitors. *Electrochim. Acta.* 2000. **45**(15–16): 2483.
3. Wang Y., Song Y., Xia Y. Electrochemical capacitors: mechanism, materials, systems, characterization and applications. *Chem. Soc. Rev.* 2016. **45**: 5925.
4. Stoller M.D., Ruoff R.S. Best practice methods for determining an electrode material's performance for ultracapacitors. *Energy Environ. Sci.* 2010. **3**: 1294.
5. Allagui A., Freeborn T.J., Elwakil A.S., Maundy B.J. Reevaluation of Performance of Electric Double-layer Capacitors from Constant-current Charge/Discharge and Cyclic Voltammetry. *Sci. Rep.* 2016. **6**: 38568.
6. International Standard IEC 62576 Electric double-layer capacitors for use in hybrid electric vehicles – Test methods for electrical characteristics.
7. Grigorchak I.I., Ponedilok G.V. *Impedance Spectroscopy: Textbook.* (Lviv: Publishing House of Lviv Polytechnic, 2011). [in Ukrainian].
8. Negroiu R., Svasta P., Pirvu C., Vasile A.I., Marghescu C. *Electrochemical impedance spectroscopy for different types of supercapacitors.* 40th International Spring Seminar on Electronics Technology (ISSE), (Aug.8, 2017, Sofia, Bulgaria) P. 1.
9. Kampouris D.K., Randviir X.Ji, E.P., Banks C. E. A new approach for the improved interpretation of capacitance measurements for materials utilised in energy storage. *RSC Adv.* 2015. **5**: 12782.
10. Itagaki M., Suzuki S., Shitanda I., Watanabe K. Electrochemical Impedance and Complex Capacitance to Interpret Electrochemical Capacitor. *Electrochemistry.* 2007. **75**(8): 649.
11. Kötz R., Hahn M., Gallay R. Temperature behavior and impedance fundamentals of supercapacitors. *Journal of Power Sources.* 2006. **154**(2): 550.
12. Bohlen O., Kowal J., Sauer D.-U. Ageing behaviour of electrochemical double layer capacitors Part I. Experimental study and ageing model. *Journal of Power Sources.* 2007 **172**(1): 468.
13. Sopčić S., Antonić D., Mandić Z., Kvastek K., Horvat-Radosević V. Single and multi-frequency impedance characterization of symmetric activated carbon single capacitor cells. *J. Electrochem. Sci. Eng.* 2018. **8**(2): 183.
14. Fletcher S., Jane Black V., Kirkpatrick I. A universal equivalent circuit for carbon-based supercapacitor. *J. Solid State Electrochem.* 2014. **18**: 1377.
15. Allagui A., Elwakil A.S., Maundy B.J., Freeborn T.J. Spectral capacitance of series and parallel combinations of supercapacitors. *ChemElectroChem.* 2016. **3**: 1429.
16. Rosli F.A., Ahmad H., Jumbri K., Abdullah A.H., Kamaruzaman S., Abdullah N.A.F. Efficient removal of pharmaceuticals from water using graphene nanoplatelets as adsorbent. *R. Soc. Open Sci.* 2021. **8**(1): 201076.
17. Patent. UA 90448C2. Maletin Y.A., Shembel O.M., Novak P.V., Pidmogilnyi S.M., Stryzhakova N.G., Izotov V.Y., Mironova A.A., Danylin V.V. Method for manufacturing electrodes with a low contact resistance for batteries and capacitors with a double electric layer. 2010. [in Ukrainian].
18. Arulepp M., Permann L., Leis J., Perkson A., Rumma K., Jänes A., Lust E. Influence of the solvent properties on the characteristics of a double layer capacitor. *Journal of Power Sources.* 2004. **133**(2): 320.
19. Lekakou C., Moudam O., Markoulidis F., Andrews T., Watts J.F., Reed G.T. Carbon-Based Fibrous EDLC Capacitors and Supercapacitors. *J. Nanotechlogy.* 2011. ID 409382.

20. Freeborn T.J., Maundy B., Elwakil A.S. Fractional-order models of supercapacitors, batteries and fuel cells: a survey. *Mater. Renewable Sustainable Energy.* 2015. **4**: 9.
21. Fouda M., Elwakil A., Radwan A., Allagui A. Power and energy analysis of fractional-order electrical energy storage devices. *Energy.* 2016. **111**: 785.
22. Halsey T.C. Frequency dependence of the double-layer impedance at a rough surface. *Phys. Rev. A.* 1987. **35**: 3512.
23. R. de Levie. On porous electrodes in electrolyte solutions: I. Capacitance effects. *Electrochimica Acta.* 1963. **8**(10): 751.
24. Lewandowski A., Olejniczak A., Galiński M., Stępniak I. Performance of carbon–carbon supercapacitors based on organic, aqueous and ionic liquid electrolytes. *Journal of Power Sources.* 2010. **195**(17): 5814.
25. Karden E., Buller S., De Doncker R.W. A frequency-domain approach to dynamical modeling of electrochemical power sources. *Electrochimica Acta.* 2002. **47**(13–14): 2347.
26. Kurzweil P. *Impedance Spectroscopy – A Powerful Tool For The Characterization Of Materials And Electrochemical Power Sources.* Proc. 14th International seminar on double-layer capacitors. (Dec. 6–8, 2004 Deerfield Beach, Fl. USA.). P. 1.